Biomedicine & Pharmacotherapy 165 (2023) 115280

Contents lists available at ScienceDirect

Biomedicine & Pharmacotherapy

journal homepage: www.elsevier.com/locate/biopha

Evaluation of acute toxicity and *in vitro* antitumor activity of a novel doxorubicin-loaded folate-coated pH-sensitive liposome

Juliana de Oliveira Silva [a,*], Renata Salgado Fernandes [a], Janaína de Alcântara Lemos [a], Geovanni Dantas Cassali [c], Adriano de Paula Sabino [b], Danyelle M. Townsend [d], Mônica Cristina Oliveira [a], André Luís Branco de Barros [b,*]

[a] Department of Pharmaceutical Products, Faculty of Pharmacy, Universidade Federal de Minas Gerais, Belo Horizonte, Minas Gerais, Brazil
[b] Department of Clinical and Toxicological Analyses, Faculty of Pharmacy, Universidade Federal de Minas Gerais, Belo Horizonte, Minas Gerais, Brazil
[c] Department of General Pathology, Institute of Biological Sciences, Universidade Federal de Minas Gerais, Belo Horizonte, Minas Gerais, Brazil
[d] Department of Drug Discovery and Biomedical Sciences, Medical University of South Carolina, Charleston, SC, United States

ARTICLE INFO

Keywords:
Cytotoxicity
Doxorubicin
Folate receptor
Liposomes
Acute toxicity

ABSTRACT

Doxorubicin (DOX) loaded liposomes have been used and studied in the last decades due to the significant decrease in DOX induced cardiac and systemic toxicity relative to administration of free drug. Therefore, new strategies are sought to improve DOX delivery and antitumor activity, while avoiding side effects. Recently, folate-coated pH-sensitive liposomes (SpHL-Fol) have been studied as a tool to enhance cellular uptake and antitumor activity of paclitaxel and DOX in breast cancer cells expressing folate receptor (FR+). However, the elucidation of folate functionalization relevance in DOX-loaded SpHL (SpHL-DOX-Fol) in different cell types (MDA-MB-231, MCF-7, and A549), as well as, the complete safety evaluation, is necessary. To achieve these objectives, SpHL-DOX-Fol was prepared and characterized as previously described. Antitumor activity and acute toxicity were evaluated *in vivo* through direct comparison of free DOX verses SpHL-DOX, a well-known formulation to reduce DOX cardiotoxicity. The obtained data are crucial to support future translational research. Liposomes showed long-term stability, suitable for biological use. Cellular uptake, cytotoxicity, and percentage of migration inhibition were significantly higher for MDA-MB-231 (FR+) treated with SpHL-DOX-Fol. In addition, SpHL-DOX-Fol demonstrated a decrease in the systemic toxic effects of DOX, mainly in renal and cardiac parameters evaluation, even using a higher dose (20 mg/kg). Collectively these data build the foundation of support demonstrating that SpHL-DOX-Fol could be considered a promising drug delivery strategy for the treatment of FR+ breast tumors.

1. Introduction

Doxorubicin (DOX) is an anthracycline widely used in the front-line treatment of breast cancer. The mechanism of action of DOX is primarily attributed to the inhibition of topoisomerase I and II activity. However, DOX treatment also leads to DNA damage and the formation of reactive oxygen species (ROS). These mechanism(s) of cell injury and death are nonspecific and occur through the activation of p53-dependent apoptosis pathways and autophagy processes in healthy and cancer cells. For this reason, the use of DOX in cancer therapy is limited by its toxic effects, mainly, cardiotoxicity [1–4]. To overcome these effects, improved drug delivery systems have been explored. Liposomes were the first nanoscale drug approved for clinical use as a strategy to reduce DOX systemic toxicity due to the modification of DOX pharmacokinetics by passive tumor targeting [5–8].

Modifications in liposome composition are emerging technologies with the goal of improved pharmacokinetics and reduced toxicity. For instance, PEGylated and pH-sensitive liposomes (SpHL) have been studied in recent years to improve specificity, mainly in combination with active targeting molecules [9–11]. Previous studies performed by our research group showed that the encapsulation of therapeutic and diagnostic molecules, including DOX, into SpHL showed an advantage to improve tumor uptake with proper pharmacokinetics and safety profile even in comparison to non-pH-sensitive Doxil®-like liposomes [12–19]. The tumor-targeted delivery leads to cellular uptake of SpHL through endocytosis. The low pH of endosomes (~ pH 6–5) triggers the drug

* Corresponding authors.
E-mail addresses: julianaoliveira.far@gmail.com (J. de Oliveira Silva), brancodebarros@yahoo.com.br, albb@ufmg.br (A.L.B. de Barros).

https://doi.org/10.1016/j.biopha.2023.115280
Received 15 May 2023; Received in revised form 12 July 2023; Accepted 29 July 2023
Available online 2 August 2023

release from the SpHL, which transposes the endosome barrier, and quickly reaches the site of action [20,21]. This pH responsiveness is attributed to dioleoylphosphatidylethanolamine (DOPE) in association with a stabilizing agent, such as cholesteryl hemisuccinate (CHEMS). When combined, these lipids can organize spontaneously in the liposomal form at physiological pH. However, in acidic conditions, the lamellar structure is destabilized, and the drug is released [12,15,22].

To optimize tumor specific uptake, several ligands could be added to the liposomes based on overexpressed molecules on the cell cancer surface, to promote specific cell uptake [23]. As an example, many tumor types, including breast cancer, have overexpression of the Folate Receptor (FR). As such, folate (Fol) is a promising molecule to coat liposomes and other nanosystems to enhance selective cancer cell binding and endocytosis in FR+ tumor cells [24–28]. Previous studies demonstrated that Fol-coating active targeting and pH-sensitive combination properties in paclitaxel-loaded Fol-coated SpHL (SpHL-Fol) led to enhance drug uptake and antitumor activity [29–31].

We previously reported the development of innovative and promising Fol-coated DOX-loaded pH-sensitive liposomes (SpHL-DOX-Fol). Using a murine 4T1 breast cancer model (FR+), we showed that SpHL-DOX-Fol increased the DOX antitumor activity and reduced the occurrence of electrocardiographic alterations, typical of DOX cardiotoxicity [32]. These results built the foundation to investigate the antitumor activity potential of this new liposomal formulation against cancer human models and the evaluation of its systemic toxicity as requirement for potential translational study in the future. Therefore, this study aims to elucidate the efficacy of SpHL-DOX-Fol antitumor activity in FR+ breast and lung (FR-) cancer by *in vitro* cell uptake and cytotoxicity assays. Additionally, the long-term stability of SpHL-DOX-Fol was determined to validate its suitability for biological analysis. The pre-clinical acute toxicity was evaluated by histological and laboratory analysis in healthy BALB/c mice, to investigate and understand the complete safety profile of these new liposomes.

2. Materials and methods

2.1. Materials

Doxorubicin hydrochloride (DOX) was donated by Eurofarma® (98,6 % of purity) (Sao Paulo, Brazil). Dioleylphosphatidylethanolamine (DOPE), distearoylphosphatidyl ethanolamine coupled with polyethyleneglycol$_{2000}$ (DSPE-PEG$_{2000}$) were purchased from Lipoid GmbH (Ludwigshafen, Germany). Polycarbonate membranes were purchased from Millipore (Billerica, USA). DSPE-PEG$_{2000}$ functionalized with folate (DSPE-PEG2000-Fol) was purchased from Nanosoft Polymers (Winston-Salem, USA). Cholesteryl hemisuccinate (CHEMS) was acquired from Sigma-Aldrich (São Paulo, Brazil). High-performance liquid chromatography (HPLC) methanol and isopropyl alcohol were obtained from Tedia Company (Ohio, USA). Dubelcco's Modified Eagle's Medium (DMEM) culture medium was acquired from Sigma-Aldrich (Sao Paulo, Brazil). Antibiotic PSA (penicillin, streptomycin, and amphotericin B) and trypsin were purchased from Invitrogen (Thermo Fisher Scientific - Sao Paulo, Brazil). Fetal bovine serum (FBS) was acquired from Gibco (Sao Paulo, Brazil). Xylazine solution (Dopaser® 2 %) was purchased from Hertape Calier (Juatuba, Brazil). Ketamine hydrochloride solution (Dopalen® 10 %) was purchased from Vetbrands Agroline (Campo Grande, Brazil). All other reagents and chemicals were acquired in analytical grade. MDA-MB-231, MCF-7, and A549 cell lines were obtained from American Type Culture Collection (ATCC® - Manassas, USA).

2.2. Preparation and physicochemical characterization of liposomes

Liposomes were prepared using the thin lipid-film hydration method and characterized by mean diameter, polydispersity index (PDI), and zeta potential as described previously [19,32].

Chloroform aliquots of DOPE, CHEMS, DSPE-PEG2000 (5.8:3.7:0.5 molar ratio, respectively; 20 mM total concentration of lipids) or DOPE, CHEMS, DSPE-PEG2000, and DSPE-PEG2000-Fol (5.8:3.7:0.5 molar ratio, respectively; 20 mM total concentration of lipids) were transferred to a round flask and the solvent was removed at 25 °C and low pressure (~100 bar) to obtain the thin lipid films of SpHL or SpHL-Fol. The lipid film was hydrated with 300 mM ammonium sulfate solution and 0.1 M NaOH solution, under vigorous stirring using a vortex, and at room temperature. The volumes of 300 mM ammonium sulfate and 0.1 M NaOH solutions were determined to reach the initial lipid concentration and ionize all CHEMS molecules, respectively. The size of the blank liposomes was calibrated by extrusion using polycarbonate membranes. Extrusion was performed in pressurized nitrogen flow using membranes with 0.4 μm, 0.2 μm, and 0.1 μm of pore size (5 cycles per membrane). The non-encapsulated ammonium sulfate was removed from SpHL and SpHL-Fol by ultracentrifugation (Ultracentrifuge Optima® L-80XP, Beckman Coulter, Brea, USA) at 150,000 x g, 4 °C, for 120 min. The pellets were redispersed using 0.9 % (w/v) NaCl solution maintaining the initial lipid concentration. Afterward, DOX powder in sufficient amount to reach 2 mg/mL was added to the blank SpHL or SpHL-Fol liposomes dispersion and incubated for 2 h at 4 °C to promote the DOX encapsulation by ammonium sulphate gradient method [33]. The non-encapsulated DOX was removed by ultracentrifugation at 150,000 x g, 4 °C, for 120 min and the pellets were resuspended again with 0.9 % (w/v) NaCl solution to obtain the final dispersion of SpHL-DOX and SpHL-DOX-Fol.

For the characterization, mean diameter and polydispersity index (PDI) were determined by dynamic light scattering (DLS) at 25 °C and an angle of 90°. Electrophoretic mobility associated with the DLS was used to obtain the zeta potential. The measurements were performed using a Zetasizer NanoZS90 equipment (Malvern Instruments, Worcestershire, UK). All samples were diluted in 0.9 % (w/v) NaCl solution at a ratio of 1:100 and the measurements were performed in triplicate.

2.2.1. Determination of DOX content in liposomes

Quantification of DOX was measured by high performance liquid chromatography (HPLC) as previously reported [32]. The mobile phase was a mixture of methanol:phosphate buffer pH 3.0 (volume ratio 65:35). The elution time was 8 min at a flow rate of 1.0 mL/min, once the retention time of DOX is close to 4 min. The analysis was performed on a model 515 pump, a model 717 Plus autoinjector, and fluorescence detector model 2475 (Waters Instruments, Milford, MA, USA) with excitation and emission wavelengths of 470 nm and 555 nm, respectively. The column (ACE® C8, 25 cm × 4.6 mm, 5 μm - Merck, Darmstadt, Germany) was maintained at room temperature, and the injection volume was 20 μL. For quantification of DOX into SpHL-DOX and SpHL-DOX-Fol, the lipid membrane was opened with isopropyl alcohol (volume ratio equal to 1:10), and then the preparation was diluted appropriately in the mobile phase to reach 40 ng/mL concentration (range of calibration curve is 20–80 ng/mL). The DOX concentration was determined in triplicate before (non-purified liposomes) and after the final ultracentrifugation (purified liposomes), and the DOX encapsulation percentage (EP) was calculated according to Eq. (1):

$$EP(\%) = \left(\frac{[DOX]\quad purified\quad liposomes}{[DOX]non-purified\quad liposome}\right)x100 \tag{1}$$

2.2.2. Liposomes stability

2.2.2.1. Storage stability. To determine the shelf-life of SpHL, SpHL-Fol, SpHL-DOX, and SpHL-DOX-Fol, the liposomes, in aqueous medium, were prepared and maintained at 4 °C and aliquots were collected after 0, 7, 14, 30, 60, 120, and 180 days of preparation. Mean diameter, PDI, and zeta potential were measured as aforementioned. At the same time interval, aliquots were collected for EP determination. To separate the aqueous phase (containing released DOX) from the liposomes, the

aliquots were submitted to an ultrafiltration method using centrifugal devices Amicon® Ultra – 50 kDa (Merck S.A., Darmstadt, Germany) pre-treated with Tween 20 5 % (v/v) solution for 24 h [34]. The released DOX (aqueous phase), as well as SpHL-DOX and SpHL-DOX-Fol before ultrafiltration (non-purified liposomes) were collected, diluted, and the concentration of DOX was measured by HPLC as described above. The EP was calculated as Eq. (2) and the measurements were performed in triplicate.

$$EP(\%) = 100 - \left(\frac{[DOX]aqueous\quad phase}{[DOX]non-purified\quad liposome}\right)x100 \tag{2}$$

2.2.2.2. In vitro biological stability. SpHL-DOX and SpHL-DOX-Fol were added in phosphate saline buffer (PBS) pH 7.4 or DMEM culture media supplemented with 10 % (v/v) of FBS to estimate liposomes behavior in biological assays (*in vitro* and *in vivo*). The liposomes were diluted in PBS or DMEM (volume ratio 1:4) and incubated at 37 °C for 24 h. An aliquot was collected before incubation and after 24 h to measure the mean diameter, PDI, and zeta potential, as previously described.

2.3. Cell Culture

The MDA-MB-231 (FR+) and MCF-7 (FR+) human breast cancer cells, and A549 (FR-) human lung cancer cells were grown in DMEM supplemented with 10 % (v/v) of FBS and 1 % (v/v) of PSA. The cell lines were kept at 37 °C and 5 % of CO_2 in a humidified atmosphere [29].

2.3.1. Cytotoxicity assay

MDA-MB-231, MCF-7, or A549 tumor cells were seeded in 96-well plates (1×10^4 cells/well) at 24 h before treatment. Cells were exposed to serial concentrations (2500–40 nM), DOX, SpHL-DOX, and SpHL-DOX-Fol for 48 h. The percentage of cell growth control was calculated using the sulforhodamine B (SRB) assay in well and plate triplicate [35]. The cells were fixed with 10 % (w/v) trichloroacetic acid (TCA) after the treatment time and dyed with SRB. To remove unbound SFB, cells were washed with 1 % (v/v) acetic acid. The complex protein-SRB was solubilized with 10 mM Tris(hydroxymethyl)amino-methane (Tris-base) solution and the resulting optical density was read at 510 nm in a Spectra Max Plus 384 microplate reader (Molecular Devices – Sunnyvale, USA). The inhibitory concentration (IC_{50}) was calculated [36].

2.3.2. Migration assay

To evaluate the bi-dimensional cell migration, MDA-MB-231, MCF-7, or A549 tumor cells were seeded in 12-well plates (3×10^5 cells/well) and incubated at 37 °C for 24 h to produce a cell monolayer. A linear wound was created in individual wells (n = 3) with a 10 μL pipette tip and images were acquired using a microscope AxioVert 25 connected to an Axio Cam MRC camera (Zeiss, Oberkochen, Germany). These images (t = 0) were used as control. After obtaining the wounds, the wells were supplemented with 1 mL of fresh DMEM with 1 % (v/v) FBS containing 500 nM of DOX, SpHL-DOX, or SpHL-DOX-Fol. The plates were incubated at 37 °C for 24 h and new images were obtained (t = 24 h). This analysis method was chosen to reduce the variation between different wells once the same scratch was photographed and the areas were calculated before and after treatment. Wound areas were obtained using the MRI Wound Healing Tool plugin for the free version of Image J 1.45 software (National Institutes of Health, Bethesda, USA). The wound healing percentage was calculated according to Eq. (3).

$$Migration(\%) = 100 - \left(\frac{treated\quad wound\quad areas}{\text{"control" wound areas}}\right)x100 \tag{3}$$

2.3.3. Cellular uptake of DOX

HPLC was used to quantify the cellular uptake of DOX from SpHL-DOX and SpHL-DOX-Fol while its intracellular uptake was visualized by confocal microscopy. To quantify DOX cellular uptake, MDA-MB-231, MCF-7, or A549 tumor cells were plated in 12-well plates (5×10^5 cells/well) and incubated for 24 h. Cells were treated (n = 3) with 1 mL of fresh DMEM containing 5 μM of DOX, SpHL-DOX, or SpHL-DOX-Fol for 1 and 4 h. Briefly, after treatment, the cells were removed from the plates, washed with PBS to remove the non-internalized drugs and centrifuged (500 x g, 5 min). Pellets were resuspended in 0.5 mL isopropyl alcohol and 0.5 mL methanol and the samples were transferred to the ultrasonic bath to promote the cell lysis and DOX extraction. The lysed cells were centrifuged at 3000 x g for 15 min and an aliquot of the supernatant was used for quantifying the intracellular DOX by HPLC as described in Section 2.2.2.2. The DOX cellular uptake was calculated by Eq. 4.

$$Cell\quad Uptake(\%) = \frac{[DOX]extracted\quad from\quad cells}{[DOX]total}\quad x100 \tag{4}$$

To visualize cellular uptake, confocal microscopy was used. MDA-MB-231 tumor cells were seeded in 6-well plates with sterile coverslips (3×10^5 cells/well) 24 h before treatment. Cells were exposed to 5 μM of DOX, SpHL-DOX, or SpHL-DOX-Fol for 1 and 4 h. Drug was removed with PBS buffer. Cells were fixed with 3.7 % (v/v) formaldehyde solution for 10 min at room temperature and permeabilized with 0.1 % (v/v) Triton X-100 solution for 10 min at room temperature [37]. Nuclei were labeled with fluorescent probe Hoechst 33258 (Thermo Fisher Scientific - Waltham, USA). The coverslips were washed with PBS puffer and slides were assembled using Prolong Gold Antifade Reagent (Thermo Fisher Scientific - Waltham, USA). Cells were analyzed in the *Centro de Aquisiç ão e Processamento de Imagens da Universidade Federal de Minas Gerais* (CAPI/UFMG – Belo Horizonte, Brazil) using the LSM 880 confocal microscope with Airyscan detector (Zeiss - Oberkochen, Germany). Images were acquired at 63x using a Diode 405 nm (excitation of Hoechst 33258) and Argonium 488 nm (excitation of DOX) [32]. The images were processed using the ZEN Blue Edition software version 2.3 lite (Zeiss - Oberkochen, Germany).

2.4. In vivo acute toxicity

The evaluation of *in vivo* acute toxicity followed OECD Guideline for Testing of Chemicals 423 (2001) recommendations adapted to intravenous drugs, as previously reported by our research group [19]. Animals were obtained from the *Centro de Bioterismo do Instituto de Ciências Biológicas da Universidade Federal de Minas Gerais* (CEBIO/UFMG - Belo Horizonte, Brazil). Healthy female BALB/c mice of 8–10 weeks and approximately 18 g were used. All *in vivo* studies were previously approved by the local ethics committee for animal use (CEUA/UFMG - Protocol n° 110/20, approval date 19 Jun 2020).

A single dose of DOX, SpHL-DOX, or SpHL-DOX-Fol (20 mg/kg) was administered intravenously, by the tail vein (n = 6/treatment group). Previous studies with similar liposomal formulations did not show toxicity related to the lipid components of vehicles and the evaluated parameters were comparable with the saline-treated animals [12,19,32]. Therefore, in this study, the mice of the control group received only saline (NaCl) 0,9 % (w/v). Following treatment, animals were observed for 7 days, to detect the peak of systemic toxic effects and 14 days, as recommended by the OECD guideline. Behavioral/clinical modifications, body weight, morbidity, and mortality were evaluated during all experimental protocols [38]. The weight variation is calculated by the difference between the final and initial weight of the animals. To estimate the maximum tolerated dose (MTD), the survival of all animals, associated with a body weight loss below 15 % during the experiment, was considered as the threshold for MTD. [39]. After 7 and 14 days, the animals were anesthetized with ketamine (80 mg/kg) and xylazine (15 mg/kg), and the blood was collected to the brachial plexus and transferred to microtubes containing an EDTA 0,1 M solution as an anticoagulant for hematological and biochemical dosages. The organs

were collected for histopathological analysis.

2.4.1. Blood chemistry analysis

Hematological parameters, such as hemoglobin, number of red blood cells (RBC), hematocrit (HCT), Red Cell Distribution Width (RDW), total white blood cells (WBC), granulocytes, non-granulocytes, and platelets were evaluated for each group. An automatic analyzer (HEMOVET 2300- Brasmed, Paulinia, Brazil) was used to measure the parameters. For clinical chemistry analysis, blood was centrifuged (1100 x g, 15 min) and the plasma obtained was frozen at − 20 °C until the tests. Analysis were performed with Bioplus BIO-2000 semiautomatic equipment (São Paulo, Brazil) using commercial kits (Labtest, Lagoa Santa, Brazil). Kidney function was evaluated by the measurement of blood urea nitrogen (BUN) and creatinine concentrations; liver function was assessed by alanine aminotransferase (ALT) and aspartate aminotransferase (AST) activity; and heart injury by the dosage of creatine kinase - MB (CK-MB) activity.

2.4.2. Histopathological analysis

For histopathological analysis, liver, kidneys, spleen, sternum, and heart were collected. Tissues were fixed in 10 % (v/v) buffered formaldehyde solution for 24 h, dehydrated with alcohol in increased concentrations and included in paraffin blocks. Using a microtome, 4 μm sections were obtained and the slides were stained with hematoxylin and eosin (H&E) using a routine protocol. The stained tissues were evaluated by trained pathologists and the images were captured by a camera connected to an optical microscope (Olympus BX-40; Olympus, Tokyo, Japan).

2.5. Statistical analysis

The obtained data were expressed as the mean ± standard deviation (SD). The normality of the variables was verified by D'Agostino test. Differences between the experimental groups were calculated by ANOVA analysis of variance followed by Tukey's test. For all analyses, the 95 % confidence interval was adopted, and the differences were considered significant when the P-value was < 0.05 ($P < 0.05$). Data were evaluated with GraphPad Prism software (version 5.00, La Jolla, USA).

3. Results

3.1. Preparation and physicochemical characterization of liposomes

The characterization parameters of the liposomes (SpHL, SpHL-Fol, SpHL-DOX, and SpHL-DOX-Fol) are shown in Table 1. Monodisperse vesicles, with mean diameter close to 100 mn and neutral superficial charge (zeta potential) were obtained, also all the formulation showed a neutral pH after preparation (7.2 ± 0.2). No significant ($P > 0.05$) variations were observed between SpHL and SpHL-Fol in terms of mean diameter, PDI, and zeta potential. An efficient encapsulation method was used once the EP reached almost 100 % for SpHL-DOX and SpHL-DOX-Fol. In addition, the DOX encapsulation and functionalization processes did not affect any of the characterization parameters.

Table 1
Mean diameter, PDI, zeta potential, and encapsulation percentage of SpHL, SpHL-Fol, SpHL-DOX, and SpHL-DOX-Fol.

	SpHL	SpHL-Fol	SpHL-DOX	SpHL-DOX-Fol
Mean Diameter (nm)	110 ± 4	108 ± 4	108 ± 2	107 ± 4
PDI	0.07 ± 0.03	0.06 ± 0.01	0.09 ± 0.03	0.10 ± 0.02
Zeta Potential (mV)	-2.8 ± 0.7	-2.5 ± 0.5	-2.4 ± 0.6	-2.6 ± 0.5
EP (%)	-	-	99.5 ± 0.3	99.6 ± 0.1
Drug Load (mg/mL)			1.92 ± 0.35	1.97 ± 0.17

Data are expressed by the mean (n = 3) ± standard deviation of the mean. All data were analyzed by one-way ANOVA analysis of variance followed by Tukey's post-test.

3.2. Liposome stability

Mean diameter, PDI, zeta potential, EP were evaluated to characterize the stability (shelf life) of SpHL-DOX and SpHL-DOX-Fol as well as the influence of functionalization in liposome physicochemical stability. Long-term stability (6 months) for both liposomes was observed with preservation of mean diameter, PDI, zeta potential, and EP (Table 2). The final mean diameter remained at about 100–110 nm and a neutral (−2 to −4 mV) superficial charge was observed for SpHL-DOX and SpHL-DOX-Fol (Figs. 1A and 1B). In addition, no notable changes ($P > 0.05$) were observed in PDI and EP, once the liposomes showed EP ~100 % and PDI < 0.1 after 6 months of storage at 4 °C (Fig. 1B) (Table 2). In addition, pH remains stable throughout the study.

The mean diameter, PDI, and zeta potential of the liposomes were evaluated again after incubation in buffer solution (PBS) or biological medium (DMEM) supplemented with 10 % (v/v) of FBS. SpHL-DOX and SpHL-DOX-Fol showed suitable stability in simulated biological conditions (pH, temperature, and protein content) for 24 h after incubation. Any significant changes ($P > 0.05$) were observed in mean diameter, zeta potential (Fig. 2), and PDI, which remained below 0.1. Therefore, liposomes could be considered suitable for *in vitro* and *in vivo* assays.

3.3. Cytotoxicity evaluation

Cytotoxicity of DOX, SpHL-DOX, and SpHL-DOX-Fol was evaluated in FR+ breast cancer cells (MDA-MB-231, MCF-7) and FR- lung cancer cells (A549). Dose-dependent cytotoxicity was observed for the free-drug (DOX) and drug-loaded liposomes (SpHL-DOX, and SpHL-DOX-Fol) (Fig. 3). For MDA-MB-231, the cytotoxicity was higher ($P < 0.05$) for SpHL-DOX-Fol in comparison with DOX and SpHL-DOX (Fig. 3A). The IC_{50} values for DOX, SpHL-DOX, and SpHL-DOX-Fol treatments were 518 ± 105 nM, 450 ± 115 nM, and 387 ± 157 nM, respectively. In contrast, no differences ($P > 0.05$), in percentage of control cell growth, were observed among DOX, SpHL-DOX, and SpHL-DOX-Fol for MCF-7 and A549 (Figs. 3B and 3C). SpHL and SpHL-Fol did not show cytotoxicity (~100 % of cell viability) or any other effects on cells, confirming that the vehicle was not toxic or active, as described previously (data not shown) [32].

3.4. Migration assay

Figs. 3D, 4 and S1 show the migration profile for cell lines MDA-MB-231, MCF-7 and A549. The wound-healing migration assay has been used to predict the influence of drug treatments on cell motility. In cancer research, this motility could be related to the metastasis process

Table 2
Physicochemical characterization of SpHL, SpHL-Fol, SpHL-DOX, and SpHL-DOX-Fol after 180 days.

	SpHL	SpHL-Fol	SpHL-DOX	SpHL-DOX-Fol
Mean Diameter (nm)	112 ± 1	110 ± 4	103 ± 2	98 ± 3
PDI	0.06 ± 0.03	0.07 ± 0.02	0.08 ± 0.03	0.07 ± 0.02
Zeta Potential (mV)	-3.5 ± 0.6	-3.8 ± 0.4	-2.8 ± 0.7	-3.7 ± 0.6
EP (%)	-	-	98.4 ± 0.4	99.5 ± 0.5

Data are expressed by the mean (n = 3) ± standard deviation of the mean. All data were analyzed by one-way ANOVA analysis of variance followed by Tukey's post-test.

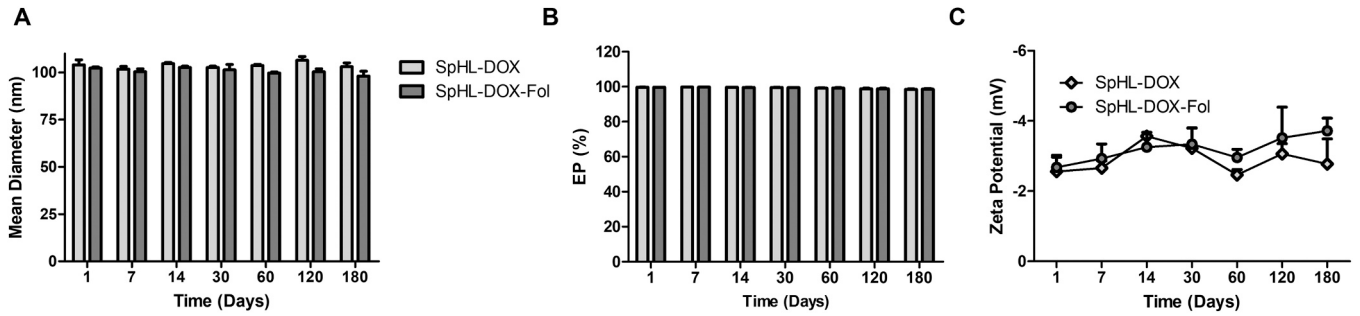

Fig. 1. Liposomes mean diameter (A), encapsulation percentage (EP) (B) and zeta potential (C) up to 180 days. Data are expressed by the mean (n = 3) ± standard deviation of the mean. All data were analyzed by one-way ANOVA analysis of variance followed by Tukey's post-test. **Represents statistical difference ($P < 0.05$) related to Day 1 for SpHL-DOX or SpHL-DOX-Fol.

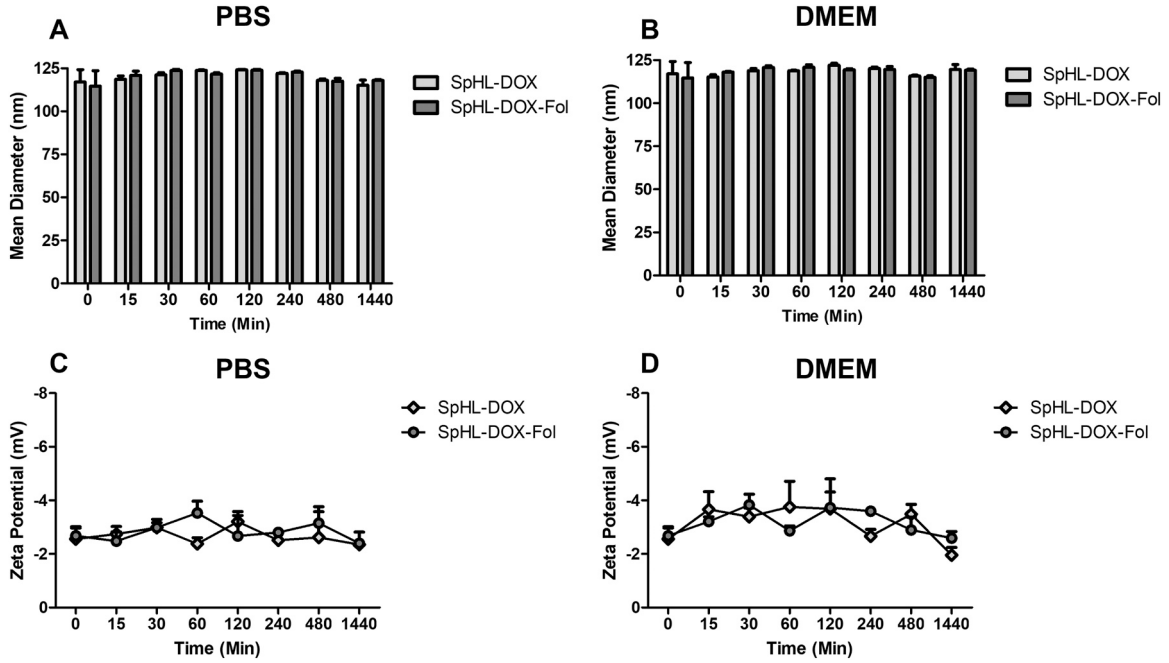

Fig. 2. Liposomes mean diameter (A and B) and zeta potential (C and D) after incubation in PBS or biological media DMEM supplemented with 10 % (v/v) of FBS for 24 h. Data are expressed by the mean (n = 3) ± standard deviation of the mean. All data were analyzed by one-way ANOVA analysis of variance followed by Tukey's post-test.

in vivo, and treatments with great potential for cell motility inhibition are desirable [40]. For MDA-MB-231, SpHL-DOX-Fol was highly efficient to inhibit cell motility. After 24 h, only 12.8 ± 8.2 % of the wound area has been healed (Figs. 3D and 4) for SPHL-DOX-Fol compared to more than 30 % for DOX and SpHL-DOX treated cells. In MCF-7 cells, a similar behavior was observed, however, the inhibition was less pronounced. In contrast, there was no statistical difference ($P > 0.05$) in cell migration in the lung cancer cells (A549) observed at 24 h after treatment with DOX, SpHL-DOX, or SpHL-DOX-Fol (Figs. 3D and S1).

3.5. Cellular uptake

The intracellular uptake of DOX from the treatments in MDA-MB-231, MCF-7, and A549 human tumor cells as well as their intracellular location in MDA-MB-231 are shown in Fig. 5. Here we show a dose-dependence increase in cellular update following exposure in MDA-MB-231for all formulations. However, there was a significant increase ($P < 0.05$) in DOX uptake from SpHL-DOX-Fol (30.1 ± 2.7 %). These data underscore the importance of active receptor target in cellular uptake of nanosystems, once the uptake of SpHL-DOX is the same or lower than the free drug (Figs. 5A and 5B). Additionally, Fig. 5C showed the nuclear DOX localization following cellular uptake. The purple color indicates the merging of DOX and DNA staining for all drug-treated cells (DOX, SpHL-DOX, SpHL-DOX-Fol) and suggests efficient DOX delivery. The nuclear localization is crucial given the primary mechanism of action of DOX is mediated through inhibition of DNA synthesis [41]. In contrast, the relative analysis using the free DOX as a comparison showed that for MCF-7 and A549 the presence of Fol on the liposome surface did not affect the uptake profile (Fig. 5A).

3.6. In vivo acute toxicity

3.6.1. Body weight, clinical parameters, and mortality

Changes in body weight following drug exposure is shown in Fig. 6A. Significant ($P < 0.05$) weight loss was observed for all drug-treated groups and weight gain for control mice. At day 7, DOX-treated mice showed weight loss of around 20 %. The pronounced weight loss was consistent with the maximum tolerated dose as led to death (Fig. 6B). For animals that received SpHL-DOX and SpHL-DOX-Fol, the weight loss was significantly ($P < 0.05$) lower than DOX-treated animals on day 7 (11 % and 14 %, respectively), and the loss was attenuated until day 14. Mortality was not observed in mice treated with SpHL-DOX-Fol and only

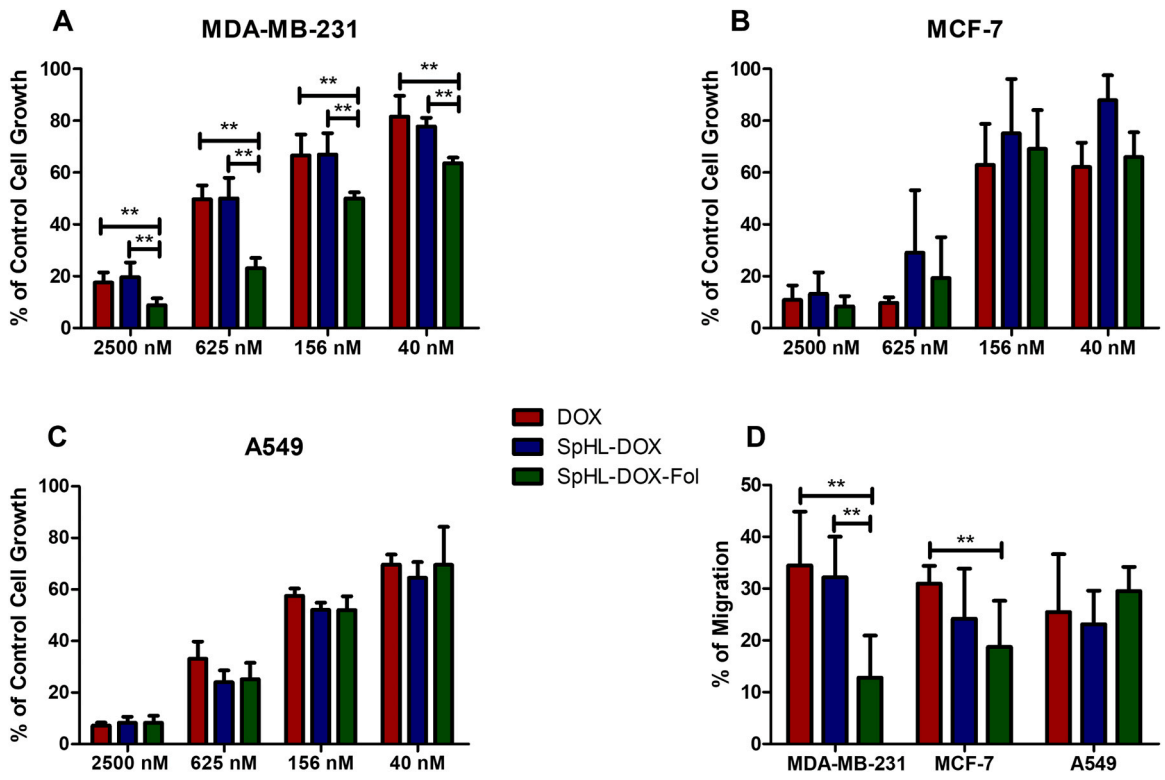

Fig. 3. Percentage of control cell growth (A, B and C) and migration percentage (D) of DOX, SpHL-DOX, and SpHL-DOX-Fol in MDA-MB-231, MCF-7, and A549 human tumor cells. Data are expressed by the mean (n = 4) ± standard deviation of the mean. All data were analyzed by one-way ANOVA analysis of variance followed by Tukey's post-test. **Represents statistical differences ($P < 0.05$) between the groups.

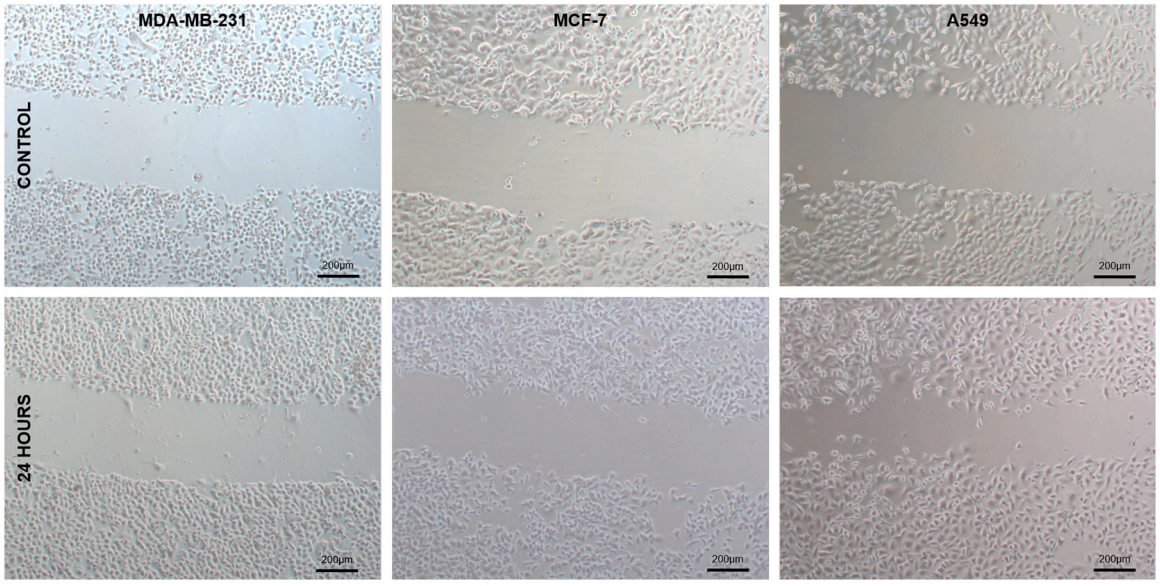

Fig. 4. Representative photomicrographs of the wounds of MDA-MB-231, MCF-7, and A549 human tumor cells before and after exposure to 500 nM of SpHL-DOX-Fol for 24 h. Images are representative of four independent experiments. Amplification of 5x.

one animal died in the SpHL-DOX group (Fig. 6B).

The most relevant clinical signs of toxicity were observed in mice treated with free drug/DOX (prostration, intense piloerection, and diarrhea). For SpHL-DOX treated mice moderate piloerection was observed in all animals and moderate to intense ascites were observed in two animals. Interestingly, the animals that received SpHL-DOX-Fol treatment showed moderate piloerection as observed for SpHL-DOX, however, just discrete ascites were observed in two. According to these results, the maximum tolerated dose (MTD) estimated for DOX was < 20 mg/kg and for liposomes (SpHL-DOX and SpHL-DOX-Fol) were close to 20 mg/kg.

3.6.2. Hematologic analysis0

A complete blood count was performed to evaluate the impact of drug treatment on hematologic factors. Blood cells parameters for the Saline, DOX, SpHL-DOX, and SpHL-DOX-Fol groups are shown in

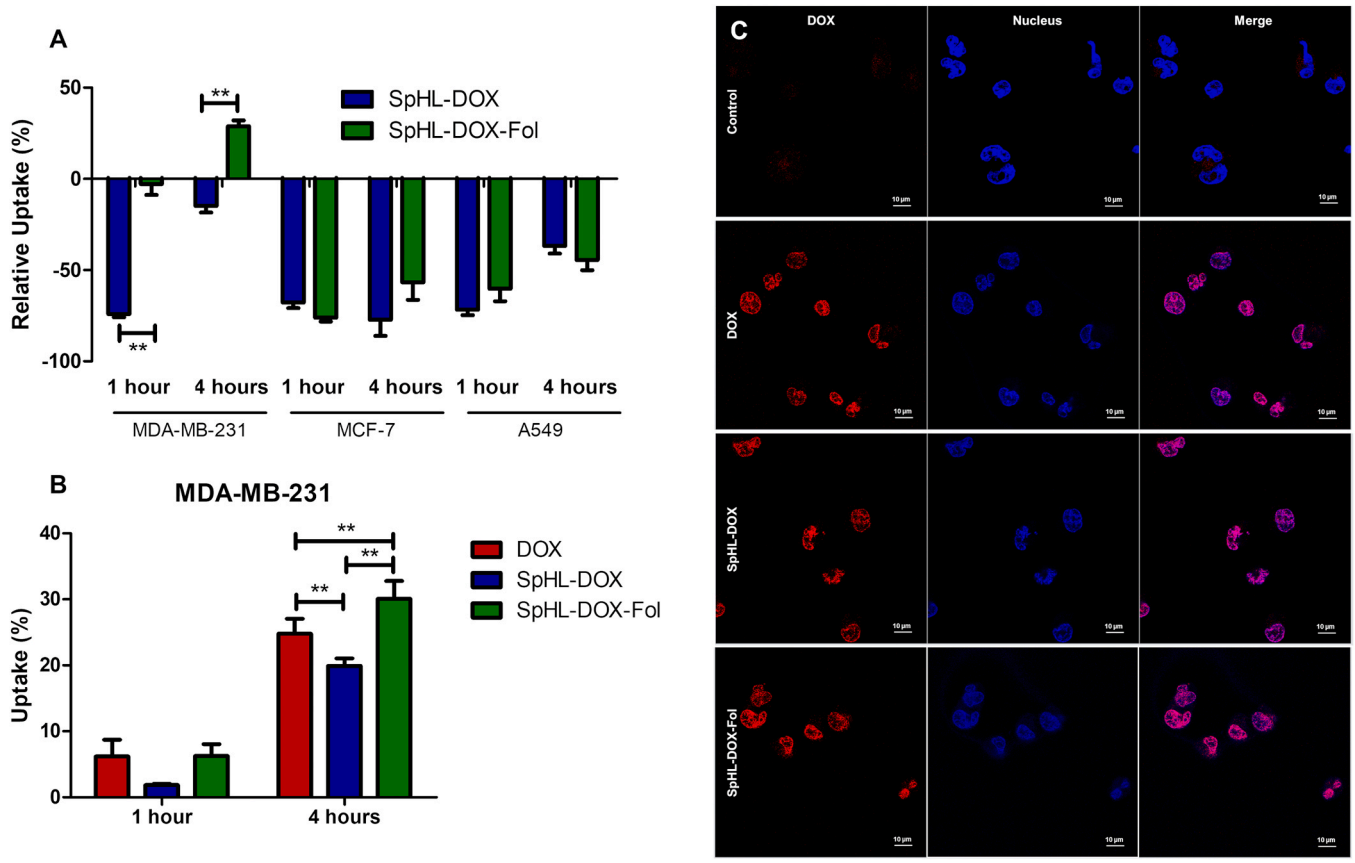

Fig. 5. Relative cell uptake of SpHL-DOX and SpHL-DOX-Fol in MDA-MB-231, MCF-7, and A549 (A), cell uptake (B), and confocal microscopy (C) of DOX, SpHL-DOX, and SpHL-DOX-Fol in MDA-MB-231. Data are expressed by the mean (n = 3) ± standard deviation of the mean. All data were analyzed by one-way ANOVA analysis of variance followed by Tukey's post-test. **Represents statistical differences ($P < 0.05$) between the groups. Amplification of 63x. The scale bar represents 10 μm.

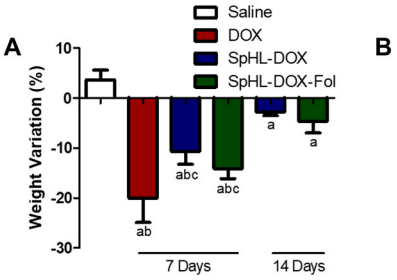

B

	Died/Tested	Day of Death
Saline	0/6	-
DOX	6/6	7,9,9,9,11,11
SpHL-DOX	1/6	13
SpHL-DOX-Fol	0/6	-

Fig. 6. Weight variation (A) and mortality (B) of BALB/c healthy female mice after treatment with Saline, DOX, SpHL-DOX, and SpHL-DOX-Fol (20 mg/kg). Data are expressed by the mean (n = 6) ± standard deviation of the mean. All data were analyzed by one-way ANOVA analysis of variance followed by Tukey's post-test. [a]Represents statistical differences ($P < 0.05$) between Saline and DOX, SpHL-DOX or SpHL-DOX-Fol. [b]Represents statistical differences ($P < 0.05$) between DOX, SpHL-DOX or SpHL-DOX-Fol at the same time of analysis. [c]Represents statistical differences ($P < 0.05$) between SpHL-DOX or SpHL-DOX-Fol at 7 and 14 days of analysis.

Table 3. The analysis of erythrocytes parameters - RBC, hemoglobin levels, HCT, RDW - were similar for all the groups at 7 and 14 days. Leukopenia was observed in all groups treated with DOX, SpHL-DOX, or SpHL-DOX-Fol on day 7 ($P < 0.05$). This alteration was characterized as a significant reduction in the non-granulocytes [19]. However, even though WBC levels for SpHL-DOX and SpHL-DOX-Fol were comparable to the control after 14 days of treatment, significant lymphopenia still was observed. Thrombocytosis occurred in DOX-treated mice on day 7.

Blood chemistry analysis was performed to assess organ toxicity (liver, kidney and heart). Biochemical parameters indicative of renal (urea and creatinine), hepatic (ALT and AST), and cardiac (CK-MB) toxicity is shown in Table 4. A significant ($P < 0.05$) increase in creatinine and urea levels was observed in animals receiving DOX on day 7. However, animals receiving SpHL-DOX or SpHL-DOX-Fol did not show signs of organ damage. This observation was similar in AST and CK-MB analysis. AST activity was significantly ($P < 0.05$) higher in DOX-treated mice compared to saline as well as to SpHL-DOX and SpHL-DOX-Fol at the same experimental time. Significant increase of CK-MB activity was observed at day 7 in animals that received DOX, however, the cardiac enzyme activity remained at normal levels in mice treated with SpHL-DOX and SpHL-DOX-Fol. On the other hand, ALT activity is increased in all treated groups.

3.6.3. *Histological analysis*

Spleen and sternal tissues were evaluated in order to observe the toxic effects of treatments in hematopoietic organs. On day 7 after treatment, was observed moderate reduction of spleen red pulp in DOX-treated animals (Fig. 7B) and for animals that received SpHL-DOX or SpHL-DOX-Fol few apoptotic foci were detected in white pulp (Figs. 7C and 7D).

Histologic analysis is consistent with the complete blood count data described above. In the sternal analysis, a reduction of bone marrow

Table 3
Hematological parameters of BALB/c healthy female mice treated with Saline, DOX, SpHL-DOX, and SpHL-DOX-Fol (20 mg/kg).

			7 Days		14 Days	
	Saline	DOX	SpHL-DOX	SpHL-DOX-Fol	SpHL-DOX	SpHL-DOX-Fol
WBC (cell/mm^3 x 10^3)	5.0 ± 0.6	1.3 ± 0.3[a]	1.1 ± 0.2[ac]	1.3 ± 0.4[ac]	4.9 ± 0.8	5.0 ± 1.5
Non-Gran (cell/mm^3 x 10^3)	3.5 ± 0.6	0.6 ± 0.1[ab]	0.6 ± 0.2[ac]	0.6 ± 0.2[ac]	2.3 ± 0.4[a]	2.5 ± 0.9[a]
Gran (cell/mm^3 x 10^3)	1.7 ± 0.2	0.7 ± 0.2[a]	0.5 ± 0.1[a]	0.7 ± 0.2[a]	2.7 ± 0.4[a]	2.5 ± 0.6[a]
RBC (cell/mm^3 x 10^6)	6.3 ± 0.4	6.7 ± 0.2	6.2 ± 0.2	6.2 ± 0.3	6.2 ± 0.1	6.1 ± 0.3
HGB (g/dL)	12.9 ± 0.8	14.1 ± 0.6	12.5 ± 0.6	12.6 ± 1.0	12.3 ± 0.4	11.9 ± 0.6
HCT (%)	31.8 ± 1.6	33.9 ± 0.7	30.9 ± 0.8	30.7 ± 1.7	30.2 ± 0.8	29.6 ± 1.4
RDW (%)	15.2 ± 0.9	16.1 ± 0.8	15.5 ± 1.0	15.2 ± 0.5	14.2 ± 0.6	14.1 ± 0.4
PLT (cell/mm^3 x 10^3)	415 ± 86	633 ± 70[a]	499 ± 94	507 ± 26	510 ± 34	519 ± 31

Data are expressed by the mean (n = 6) ± standard deviation of the mean. All data were analyzed by one-way ANOVA analysis of variance followed by Tukey's post-test. [a]Represents statistical differences ($P < 0.05$) between Saline and DOX, SpHL-DOX or SpHL-DOX-Fol. [b]Represents statistical differences ($P < 0.05$) between DOX, SpHL-DOX, or SpHL-DOX-Fol at the same time of analysis. [c]Represents statistical differences ($P < 0.05$) between SpHL-DOX or SpHL-DOX-Fol at 7 and 14 days of analysis.

Table 4
Biochemical parameters of BALB/c healthy female mice treated with Saline, DOX, SpHL-DOX, and SpHL-DOX-Fol (20 mg/kg).

			7 Days		14 Days	
	Saline	DOX	SpHL-DOX	SpHL-DOX-Fol	SpHL-DOX	SpHL-DOX-Fol
Creatinine (mg/dL)	0.39 ± 0.08	0.64 ± 0.08[ab]	0.34 ± 0.04	0.32 ± 0.04	0.37 ± 0.02	0.34 ± 0.07
Urea (mg/dL)	54 ± 7	179 ± 37[ab]	50 ± 4	51 ± 13	47 ± 13	46 ± 7
ALT (U/L)	34 ± 3	72 ± 25[a]	65 ± 9[a]	69 ± 15[a]	75 ± 17[a]	51 ± 11[a]
AST (U/L)	81 ± 8	198 ± 69[ab]	102 ± 24	114 ± 24	106 ± 18	86 ± 18
CK-MB (U/L)	38 ± 8	91 ± 38[ab]	43 ± 8	47 ± 6	35 ± 8	40 ± 7

Data are expressed by the mean (n = 6) ± standard deviation of the mean. All data were analyzed by one-way ANOVA analysis of variance followed by Tukey's post-test. [a]Represents statistical differences ($P < 0.05$) between Saline and DOX, SpHL-DOX or SpHL-DOX-Fol. [b]Represents statistical differences ($P < 0.05$) between DOX, SpHL-DOX, or SpHL-DOX-Fol at the same time of analysis. [c]Represents statistical differences ($P < 0.05$) between SpHL-DOX or SpHL-DOX-Fol at 7 and 14 days of analysis.

parenchyma was observed for all treated groups (DOX, SpHL-DOX, and SpHL-DOX-Fol) at day 7 (Figs. 8B, 8C, and 8D), characterized by replacement of functional cells for adipose tissue. It is important to note that all toxic effects described for spleen and bone marrow for SpHL-DOX or SpHL-DOX-Fol-treated animals were reversible, once the histological features of these animals at day 14 are comparable to the healthy animals (Figs. 8A, 8E, and 8F).

In hepatic histology analysis, animals treated with DOX at day 7 presented multifocal hydropic degeneration, characterized by vacuoles in hepatocytes with loss of liver architectural pattern (Fig. 9B). On the other hand, alterations were not observed in SpHL-DOX and SpHL-DOX-Fol groups at the same time interval (Figs. 9C and 9D). This is consistent with blood chemistry analysis (ALT/AST). After 14 days, these groups developed multifocal hydropic degeneration, however, without necrosis evidence (Figs. 9E and 9F).

Figs. 10 and 11 shows heart and kidney photomicrographs. As expected, small foci of discreet vacuolization were observed in cardiac muscle for all liposome-treated animals (Figs. 10C, 10D, 10E, and 10F). For DOX-treated animals, extensive foci of vacuolization with occasional areas of calcification were detected (Fig. 10B).

DOX induced kidney toxicity measured by urea and creatinine were support in histologic analysis. In Fig. 11B, renal damage was observed and depicted as accumulation of hyaline material in renal tubules (hyaline cylinders) along with glomerular sclerosis in different stages (mesangial thickening to hyaline accumulation in glomerulus). As in liver analysis, in liposome-treated the presence of toxic effects was time-dependent. On day 7 after treatment, SpHL-DOX-treated animals presented areas of cylinders and after 14 days, there was an increase in the affected area, associated with discreet mesangial thickening (Figs. 11C and 11E). Interestingly, the renal toxic effects were less evident in animals who received SpHL-DOX-Fol. On day 7, the features were comparable to saline-treated animals (Fig. 11D) and, on day 14, focal areas of hyaline cylinders were observed, however, the glomerulus morphology was preserved (Fig. 11F).

4. Discussion

Stability studies are relevant in liposome development due to the potential for physical and chemical stability problems [42]. Fusion and aggregation of vesicles are measured by the increase of the mean diameter and PDI being typical signals of liposome instability. Avoiding this phenomenon is highly desirable, once the fusion and aggregation of particles can promote the release of encapsulated content and decrease blood half-life [43]. PEG-coating liposomes have been the main strategy for conferring liposomes *in vitro* and *in vivo* stability. The PEG chains will produce a hydrophilic layer on the vesicle surface, impairing the aggregation/fusion process by steric repulsion [44–46]. In this study, PEG_{2000}-coated SpHL-DOX and SpHL-DOX-Fol were prepared and characterized by robust and reproducible methods [32]. This functionalization conferred storage stability for the formulations for 6 months in terms of mean diameter, PDI, zeta potential, and EP. Additionally, these liposomes were stable at simulated biological conditions and, therefore, suitable for *in vitro* and *in vivo* assays.

Since the beginning of nano-scale drug application in cancer therapy, strategies to promote drug accumulation into tumor cells with the purpose of decreasing systemic toxicity and enhancing antitumor activity have been investigated [47]. In this context, the Fol-coating nanosystems have been described. Folate receptor (FR) expression is weak in healthy tissues however, almost 50 % of breast tumors overexpress FR, allowing the use of a specific targeting approach [27,48,49]. In this study, we developed Fol-coated, pH-sensitive liposome (SpHL-DOX-Fol), and the cytotoxicity, migration percentage, and DOX cellular uptake were evaluated in different cell lines The effectiveness of Fol functionalization was demonstrated previously by a competition assay using an excess of free-FA. The presence of free-FA statistically reduced the cytotoxicity of SpHL-DOX-Fol [32]. The human breast tumor cell lines MDA-MB-321 (FR+) and MCF-7 (FR+), and the human lung tumor cell line A549 (RF-) were used to evaluate the advantages of the Fol-coating strategy [29,50–52]. The use of Fol-coated nanostructures aims to enhance the specific endocytosis and intracellular drug delivery in overexpressed-FR cells [27]. Cellular uptake, cytotoxicity, and inhibition of cell migration for SpHL-DOX-Fol were significantly higher in

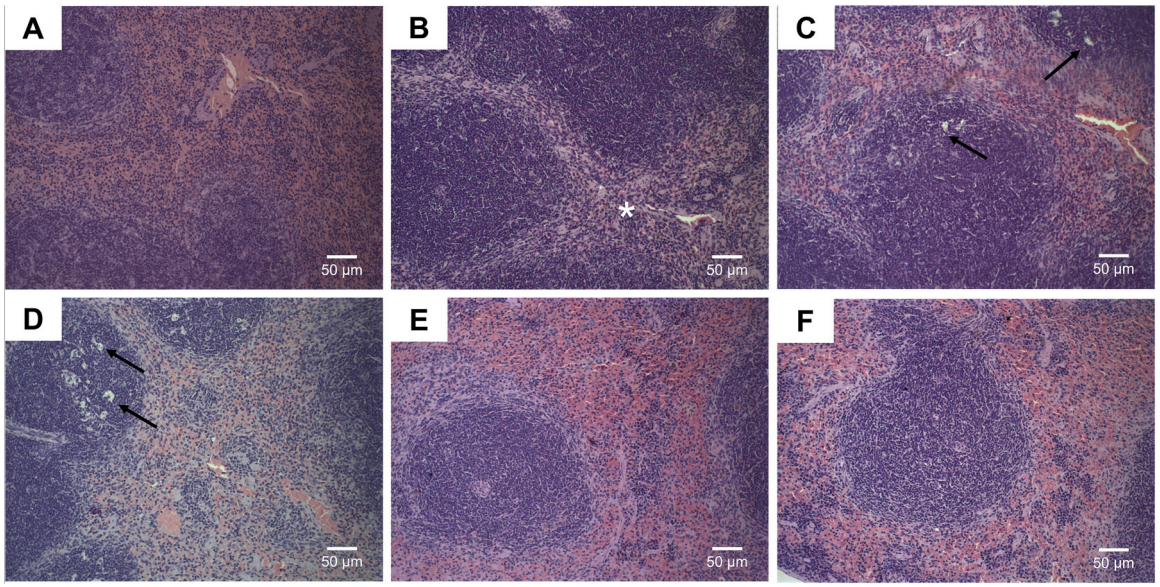

Fig. 7. Histological sections of spleen from BALB/c healthy female mice treated with Saline, DOX, SpHL-DOX, and SpHL-DOX-Fol (20 mg/kg) stained by hematoxylin & eosin. (A) Saline spleen (B) DOX spleen on day 7. (C) SpHL-DOX spleen on day 7. (D) SpHL-DOX-Fol spleen on day 7. (E) SpHL-DOX spleen on day 14. (F) SpHL-DOX-Fol spleen on day 14. White asterisk indicates red pulp hypoplasia. Black arrows indicate apoptosis. Amplification of 20x.

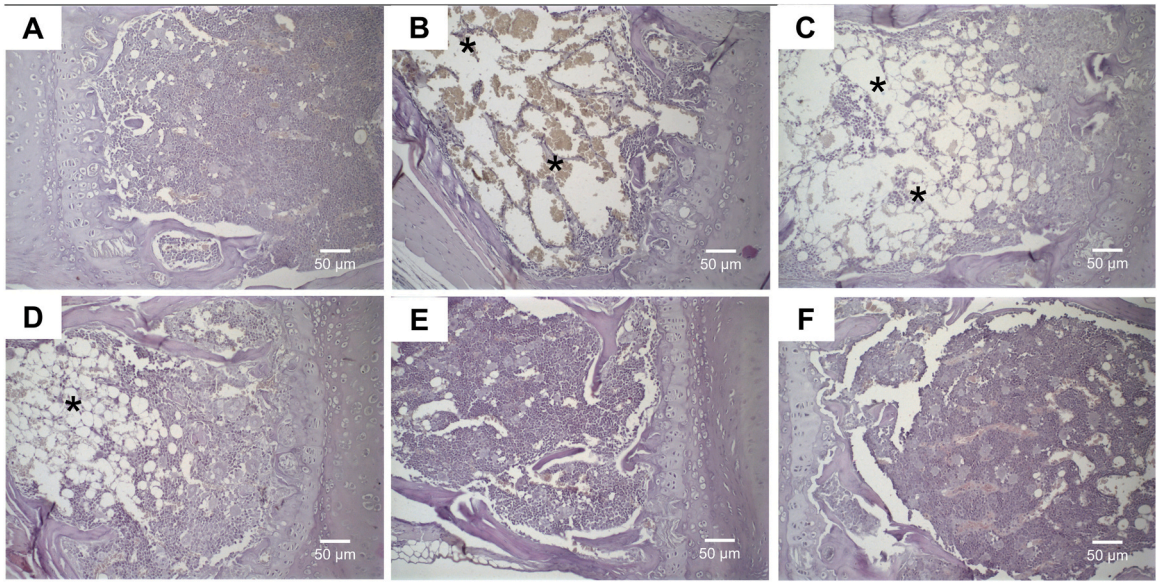

Fig. 8. Histological sections of sternum from BALB/c healthy female mice treated with Saline, DOX, SpHL-DOX, and SpHL-DOX-Fol (20 mg/kg) stained by hematoxylin & eosin. (A) Saline sternum. (B) DOX sternum on day 7. (C) SpHL-DOX sternum on day 7. (D) SpHL-DOX-Fol sternum on day 7. (E) SpHL-DOX sternum on day 14. (F) SpHL-DOX-Fol sternum on day 14**.** Black asterisks indicate adipose tissue area. Amplification of 20x.

MDA-MB-231 cells, and the intracellular percentage of DOX in this group increases in a time-dependent manner. MDA-MB-231 is described as a strongly overexpressing of FR cell line, while the receptor-expressing is mild in MCF-7 cell surface and absent in A549. These characteristics encourage the extensive use of these cell lines to evaluate the Fol-coated nanostructure's effectiveness [29,50,53–56] and evidence the crucial role of FR expression for enhancing antitumor activity of Fol-functionalized nanostructures, as SpHL-DOX-Fol.

pH-sensitive liposomes have been described as a feasible tool to deliver DOX to the tumor with a suitable safety profile, reducing the DOX cardiac and systemic toxicity [17–19]. Despite the FR's low expression in healthy cells, this is a constitutive receptor in several tissues (kidney, spleen, bone marrow, bladder, thyroid, and colon) [48,49]. Therefore, due to the important role of Fol in normal metabolism [57], studies to determine the influence of liposome functionalization in safety profile are desirable.

The most concerning DOX side effect is cardiotoxicity. The acute cardiotoxicity of DOX is characterized by degeneration of cardiomyocytes associated with electrocardiographic disturbs (QT and QTc interval prolongation) and leakage of cardiac markers, such as CK-MB, in the plasma after cardiomyocytes injury. [58,59]. SpHL-DOX and SpHL-DOX-Fol prevented the increase in CK-MB levels despite discreet cardiomyocytes vacuolization. These results corroborate with a previous study performed by our research group that described a decrease in QT and QTc alterations using SpHL-DOX and SpHL-DOX-Fol at the same cumulative dose (20 mg/kg) in tumor-bearing mice model [32]. After the DOX cardiotoxicity, myelotoxicity is the most common toxic effect in therapies using chemotherapeutic agents, even in a liposomal form [3,

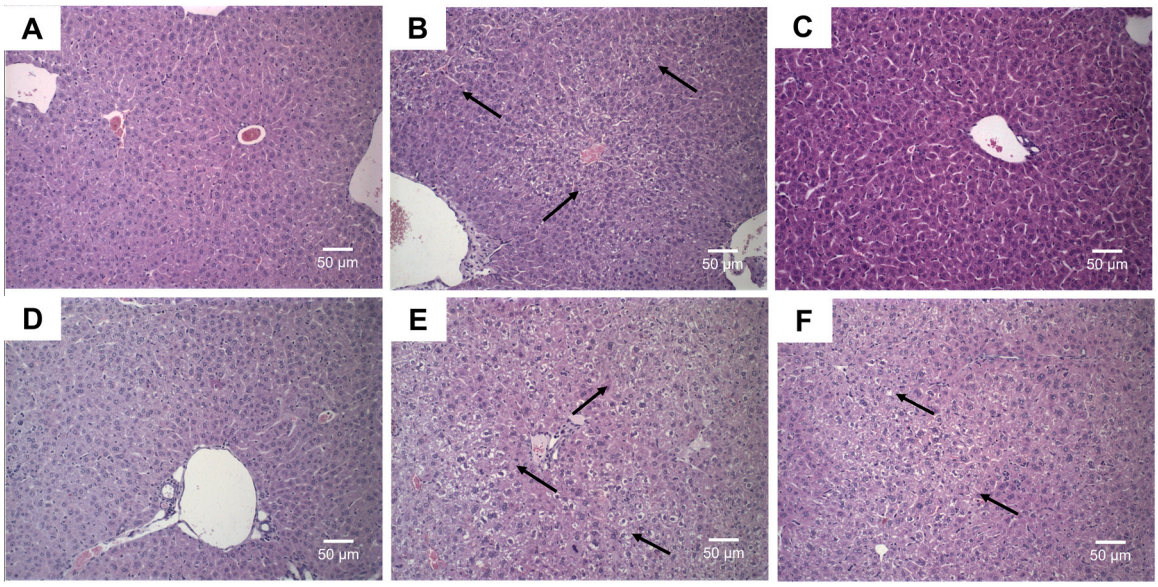

Fig. 9. Histological sections of liver from BALB/c healthy female mice treated with Saline, DOX, SpHL-DOX, and SpHL-DOX-Fol (20 mg/kg) stained by hematoxylin & eosin. (A) Saline liver. (B) DOX liver on day 7. (C) SpHL-DOX liver on day 7. (D) SpHL-DOX-Fol liver on day 7. (E) SpHL-DOX liver on day 14. (F) SpHL-DOX-Fol liver on day 14. Black arrows indicate hydropic degeneration areas. Amplification of 20x.

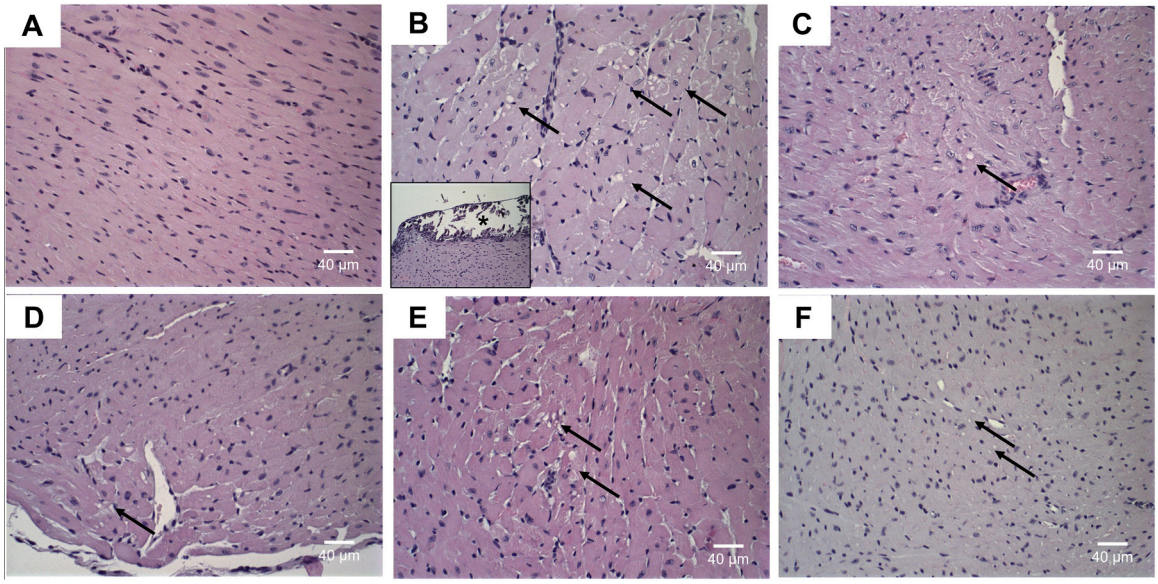

Fig. 10. Histological sections of heart from BALB/c healthy female mice treated with Saline, DOX, SpHL-DOX, and SpHL-DOX-Fol (20 mg/kg) stained by hematoxylin & eosin. (A) Saline heart. (B) DOX heart on day 7 (Inset: cardiac calcification). (C) SpHL-DOX heart on day 7. (D) SpHL-DOX-Fol heart on day 7. (E) SpHL-DOX heart on day 14. (F) SpHL-DOX-Fol heart on day 14. Black arrows indicate cardiomyocyte vacuolization area. Black asterisks indicate calcification. Amplification of 40x.

58].

Accumulation of DOX in bone marrow after treatment with DOX, SpHL-DOX, and SpHL-DOX might result in fast and intense medullar depletion leading to a significant reduction of circulating WBC on day 7 [60]. However, for SpHL-DOX and SpHL-DOX-Fol, despite the persistent lymphopenia, the effects of treatment in peripheral blood and bone marrow were reversible. Persistent lymphopenia is an expected effect after massive myelosuppression, once lymphocytes (main non-granulocyte) are predominant in mice. Additionally, in mice, the spleen remains as a hematopoietic organ in adults and the alterations in this organ can contribute to the presence of cells in peripheral blood [61].

DOX hepatotoxicity is described in acute and sub-acute doses due to partial hepatobiliary elimination and liver metabolization [62,63], and when encapsulated into liposomes, the increase of DOX hepatotoxicity may be monitored due to usual liposome uptake by the liver [14,30]. Liver injury can be observed in clinical, biochemical, and histological evaluation [19,59,64]. In this study, liver toxicity was characterized by ascites, persistent increase in aminotransferases, and hepatocyte degeneration and was observed in DOX, SpHL-DOX, and SpHL-DOX-Fol-treated animals.

Biochemical analysis showed a significant increase in creatinine and urea plasmatic levels after DOX treatment, followed by extensive renal tissue injury. DOX is a well-known inducer of kidney damage, characterized by the progressive hyaline accumulation in the glomerulus (glomerulosclerosis) with functional alteration, detected by an increase

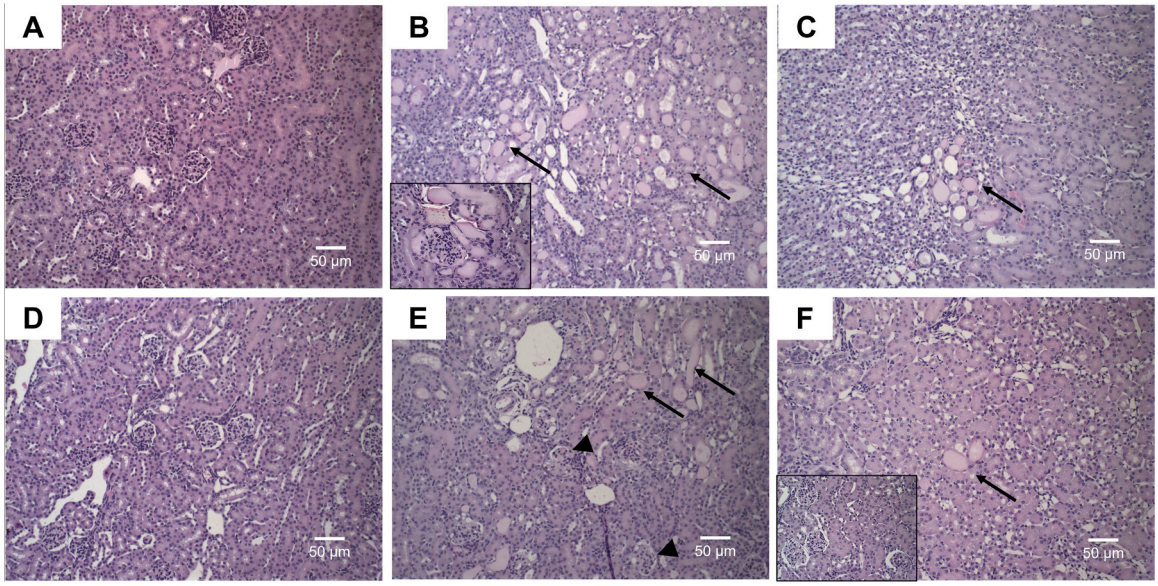

Fig. 11. Histological sections of kidney from BALB/c healthy female mice treated with Saline, DOX, SpHL-DOX, and SpHL-DOX-Fol (20 mg/kg) stained by hematoxylin & eosin. (A) Saline kidney. (B) DOX kidney on day 7 (Inset: hyaline accumulation in glomerulus). (C) SpHL-DOX kidney on day 7. (D) SpHL-DOX-Fol kidney on day 7. (E) SpHL-DOX kidney on day 14. (F) SpHL-DOX-Fol kidney on day 14 (Inset: preserved glomerulus). Black arrows indicate hyaline cylinders. Black arrowheads indicate mesangial thickening. Amplification of 20x.

in the plasmatic levels of creatinine and urea [65,66,67]. On the other hand, animals receiving SpHL-DOX and SpHL-DOX-Fol developed discreet nephrotoxicity signals in histology after 7 and 14 days, without evidence of functional alterations. Bioactive molecules mainly eliminated by renal pathway, such as DOX, have pharmacokinetics profile strongly modified when entrapped into liposomes, decreasing the free-drug renal injury occurrence even in high doses [12,17,19,68].

5. Conclusions

In this study, SpHL-DOX-Fol was prepared and characterized. The long-term shelf-life and *in vitro* biological stability showed the suitability of SpHL-DOX-Fol for biological studies. The folate-coating of liposome presented a significant advantage when used in the MDA-MB-231 (FR+) cell line, in comparison with DOX and SpHL-DOX, increasing the DOX cellular uptake and consequently, reducing the tumor cell viability and its migratory percentage in approximately 20 %. Furthermore, SpHL-DOX-Fol showed dramatic alteration in free-DOX safety profile, due to a decrease in morbimortality and hematological, cardiac, renal, and hepatic toxicity, without evidence of exacerbation of toxicity compared to SpHL-DOX. In conclusion, supported by present and previous results, that showed proper pharmacokinetic profile and significant *in vivo* tumor growth control and metastasis, SpHL-DOX-Fol could be a promising strategy to, safely, deliver DOX into FR+ breast tumors and potentially reduce metastasis occurrence.

Ethics statement

All *in vivo* studies were previously approved by the local ethics committee for animal use (CEUA/UFMG - Protocol n° 110/20, approval date 19 Jun 2020).

Funding support

This work was supported by Fundação de Amparo à Pesquisa do Estado de Minas Gerais (FAPEMIG - Brazil), Conselho Nacional de Desenvolvimento Científico e Tecnológico (CNPq - Brazil), and Coordenação de Aperfeiçoamento de Pessoal de Nível Superior (CAPES - Brazil). DMT is supported by the SC-Redox COBRE.

CRediT authorship contribution statement

Juliana O. Silva: Conceptualization, Investigation, Data Analysis, Writing – Original Draft, **Renata S. Fernandes**: Investigation, Data Analysis, **Janaína A. Lemos**: Investigation, Data Analysis, **Giovanni Dantas Cassali**: Data Analysis, **Adriano P. Sabino**: Data Analysis, **Danyelle M. Townsend**: pharmacokinetic and toxicology data analysis and writing, **Mônica C. Oliveira**: Resources, Conceptualization, Data Analysis, **André L. B. Barros**: Conceptualization, Resources, Data Analysis, Writing – Review and Editing, Supervision.

Declaration of Competing Interest

The authors declare that they have no conflict of interest.

Data availability

Data will be made available on request.

Acknowledgements

The authors would like to thank Centro de Aquisição e Processamento de Imagens da UFMG (CAPI/UFMG - Brazil) for the confocal microscopy images acquisition.

Appendix A. Supporting information

Supplementary data associated with this article can be found in the online version at doi:10.1016/j.biopha.2023.115280.

References

[1] J. Wojtacki, E. Lewicka-Nowak, K. Leśniewski-Kmak, Anthracycline-induced cardiotoxicity: clinical course, risk factors, pathogenesis, detection and prevention–review of the literature, Med. Sci. Monit. 6 (2000) 411–420.
[2] S. Zhang, X. Liu, T. Bawa-Khalfe, L. Lu, L. Yi, L.F. Liu Lyu, E.T.H. Yeh, Identification of the molecular basis of doxorubicin-induced cardiotoxicity, Nat. Med. 18 (2012) 1639–1642, https://doi.org/10.1038/nm.2919.
[3] R.M. Damiani, D.J. Moura, C.M. Viau, R.A. Caceres, J.A.P. Henriques, J. Saffi, Pathways of cardiac toxicity: comparison between chemotherapeutic drugs

doxorubicin and mitoxantrone, Arch. Toxicol. 90 (2016) 2063–2076, https://doi.org/10.1007/s00204-016-1759-y.
[4] P. Spallarossa, N. Maurea, C. Cadeddu, R. Madonna, D. Mele, I. Monte, G. Novo, P. Pagliaro, A. Pepe, C.G. Tocchetti, C. Zito, G. Mercuro, A recommended practical approach to the management of anthracycline-based chemotherapy cardiotoxicity: an opinion paper of the working group on drug cardiotoxicity and cardioprotection, Italian Society of Cardiology, J. Cardiovasc. Med. 1 (2016) 84–92, https://doi.org/10.2459/JCM.0000000000000381.
[5] A. Gabizon, H. Shmeeda, Y. Barenholz, Pharmacokinetics of pegylated liposomal Doxorubicin: review of animal and human studies, Clin. Pharmacokinet. 42 (2003) 419–436, https://doi.org/10.2165/00003088-200342050-00002.
[6] T.M. Allen, P.R. Cullis, Liposomal drug delivery systems: from concept to clinical applications, Adv. Drug. Deliv. Rev. 65 (2013) 36–48, https://doi.org/10.1016/j.addr.2012.09.037.
[7] D.R. Khan, M.N. Webb, T.H. Cadotte, M.N. Gavette, Use of targeted liposome-based chemotherapeutics to treat breast cancer, Breast Cancer 9 (2015) 1–5, https://doi.org/10.4137/BCBCR.S29421.
[8] S. Al-Mahmood, J. Sapiezynski, O.B. Garbuzenko, T. Minko, Metastatic and triple-negative breast cancer: challenges and treatment options, Drug. Deliv. Transl. Res. 8 (2018) 1483–1507, https://doi.org/10.1007/s13346-018-0551-3.
[9] A. Jain, S.K. Jain, Stimuli-responsive smart liposomes in cancer targeting, Curr. Drug. Targets 19 (2018) 259–270, https://doi.org/10.2174/1389450117666160208144143.
[10] S.S. Nunes, S.E.M. Miranda, J.O. Silva, R.S. Fernandes, J.A. Lemos, C.A. Ferreira, D. M. Townsend, G.D. Cassali, M.C. Oliveira, A.L.B. Barros, pH-responsive and folate-coated liposomes encapsulating irinotecan as an alternative to improve efficacy of colorectal cancer treatment, Biomed. Pharmacother. 144 (2021), 112371, https://doi.org/10.1016/j.biopha.2021.112317.
[11] B. Yang, B. Song, S. Shankar, A. Guller, W. Deng, Recent advances in liposome formulations for breast cancer therapeutics, Cell. Mol. Life. Sci. 78 (2021) 5225–5243, https://doi.org/10.1007/s00018-021-03850-6.
[12] E.A. Leite, A.M.Q. Lana, A.D. Carvalho-Junior, L.G.V. Coelho, M.C. Oliveira, Acute toxicity study of cisplatin loaded long-circulating and pH-sensitive liposomes administered in mice, J. Biomed. Nanotechnol. 8 (2012) 229–239, https://doi.org/10.1166/jbn.2012.1388.
[13] E.A. Leite, C.M. Souza, A.D. Carvalho-Júnior, L.G.V. Coelho, A.M.Q. Lana, G. D. Cassali, M.C. Oliveira, Encapsulation of cisplatin in long-circulating and pH-sensitive liposomes improves its antitumor effect and reduces acute toxicity, Int. J. Nanomed. 7 (2012) 5259–5269, https://doi.org/10.2147/IJN.S34652.
[14] D.C.F. Soares, V.N. Cardoso, A.L.B. Barros, C.M. Souza, G.D. Cassali, M.C. Oliveira, G.A. Ramaldes, Antitumoral activity and toxicity of PEG-coated and PEG-folate-coated pH-sensitive liposomes containing ^{159}Gd-DTPA-BMA in Ehrlich tumor bearing mice, Eur. J. Pharm. Sci. 45 (2012) 58–64, https://doi.org/ 10.1016/j.ejps.2011.10.018.
[15] A.L.B. Barros, L.G. Mota, D.C.F. Soares, C.M. Souza, G.D. Cassali, M.C. Oliveira, V. N. Cardoso, Long-circulating, pH-sensitive liposomes versus long-circulating, non-pH-sensitive liposomes as a delivery system for tumor identification, J. Biomed. Nanotechnol. 9 (2013) 1636–1643, https://doi.org/10.1166/jbn.2013.1649.
[16] F.N. Carlesso, R.S. Araújo, L.L. Fuscaldi, S.E.M. Miranda, D. Rubello, C.S. Teixeira, D.C. Reis, E.A. Leite, J.N. Silveira, S.O.A. Fernandes, G.D. Cassali, M.C. Oliveira, P. M. Colletti, A.L.B. Barros, V.N. Cardoso, Preliminary data of the antipancreatic tumor efficacy and toxicity of long-circulating and pH-sensitive liposomes containing cisplatin, Nucl. Med. Commun. 37 (2016) 727–734, https://doi.org/10.1097/MNM.0000000000000505.
[17] J.O. Silva, R.S. Fernandes, S.C.A. Lopes, V.N. Cardoso, E.A. Leite, G.D. Cassali, M. C. Marzola, D. Rubello, M.C. Oliveira, A.L.B. Barros, pH-sensitive, long-circulating liposomes as an alternative tool to deliver doxorubicin into tumors: a feasibility animal study, Mol. Imaging Biol. 18 (2016) 898–904, https://doi.org/10.1007/s11307-016-0964-7.
[18] D.S. Ferreira, B.L.J.O. Pinto, V. Kumar, V.N. Cardoso, S.O. Fernandes, C.M. Souza, G.D. Cassali, A. Moore, D.E. Sosnovik, C.T. Farrar, E.A. Leite, R.J. Alves, M. C. Oliveira, A.R. Guimarães, P. Caravan, Evaluation of antitumor activity and cardiac toxicity of a bone-targeted ph-sensitive liposomal formulation in a bone metastasis tumor model in mice, Nanomedicine 13 (2017) 1693–1701, https://doi.org/10.1016/j.nano.2017.03.005.
[19] J.O. Silva, S.E.M. Miranda, E.A. Leite, A.P. Sabino, K.B.G. Borges, V.N. Cardoso, G. D. Cassali, A.G. Guimarães, M.C. Oliveira, A.L.B. Barros, Toxicological study of a new doxorubicin-loaded pH-sensitive liposome: a preclinical approach, Toxicol. Appl. Pharmacol. 352 (2018) 162–169, https://doi.org/ 10.1016/j.taap.2018.05.037.
[20] D.S. Ferreira, S.C.A. Lopes, M.S. Franco, M.C. Oliveira, pH-sensitive liposomes for drug delivery in cancer treatment, Ther. Deliv. 4 (2013) 1099–1123, https://doi.org/10.4155/tde.13.80.
[21] M.A. Aghdam, R. Bagheri, J. Mosafer, B. Baradaran, M. Hashemzaei, A. Baghbanzadeh, M. Guardia, A. Mokhtarzadeh, Recent advances on thermosensitive and pH-sensitive liposomes employed in controlled release, J. Control. Release 351 (2019) 1–22, https://doi.org/ 10.1016/j.jconrel.2019.09.018.
[22] M.C. Oliveira, V. Boutet, E. Fattal, D. Boquet, J.M. Grognet, P. Couvreur, J. R. Deverre, Improvement of in vivo stability of phosphodiester oligonucleotide using anionic liposomes in mice, Life Sci. 67 (2000) 1625–1637, https://doi.org/10.1016/s0024-3205(00)00745-1.
[23] M. Alavi, M. Hamidi, Passive and active targeting in cancer therapy by liposomes and lipid nanoparticles, Drug. Metab. Pers. Ther. 34 (1) (2019) 8, https://doi.org/10.1515/dmpt-2018-0032.
[24] C. Chen, H. Hu, M. Qiao, X. Zhao, Y. Wang, K. Chen, X. Guo, D. Chen, Tumor-targeting and pH-sensitive lipoprotein-mimic nanocarrier for targeted intracellular delivery of paclitaxel, Int. J. Pharm. 480 (2015) 116–127, https://doi.org/10.1016/j.ijpharm.2015.01.036.
[25] Y. Yang, N. Li, Y. Nie, M. Sheng, D. Yue, G. Wang, J.Z. Tang, Z. Gu, Folate-modified poly(malic acid) graft polymeric nanoparticles for targeted delivery of doxorubicin: synthesis, characterization and folate receptor expressed cell specificity, J. Biomed. Nanotechnol. 11 (2015) 1628–1639, https://doi.org/https://doi.org/10.1166/jbn.2015.2132.
[26] J. Hong, Z. Sun, Y. Li, Y. Guo, Y. Liao, M. Liu, X. Wang, Folate-modified Annonaceous acetogenins nanosuspensions and their improved antitumor efficacy, Int. J. Nanomed. 12 (2017) 5053–5067, https://doi.org/10.2147/IJN.S134284.
[27] M. Alibolandi, K. Abnous, F. Hadizadeh, S.M. Taghdisi, F. Alabdollah, M. Mohammadi, H. Nassirli, M. Ramezani, Dextran-poly lactide-co-glycolide polymersomes decorated with folate-antennae for targeted delivery of docetaxel to breast adenocarcinima in vitro and in vivo, J. Control. Release 241 (2016) 45–56, https://doi.org/10.1016/j.jconrel.2016.09.012.
[28] A. Ahmad, F. Khan, R.K. Mishra, R. Khan, Precision cancer nanotherapy: evolving role of multifunctional nanoparticles for cancer active targeting, J. Med. Chem. 62 (2019) 10475–10496, https://doi.org/10.1021/acs.jmedchem.9b00511.
[29] M.V. Barbosa, L.O.F. Monteiro, G. Carneiro, A.R. Malagutti, J.M.C. Vilela, M. S. Andrade, M. C. O, A.D. Carvalho-Junior, E.A. Leite, Experimental design of a liposomal lipid system: a potential strategy for paclitaxel-based breast cancer treatment, Colloids Surf. B Biointerfaces 163 (2015) 553–561, https://doi.org/10.1016/j.colsurfb.2015.09.055.
[30] L.O.F. Monteiro, R.S. Fernandes, C.M.R. Oda, S.C. Lopes, D.M. Townsend, V. N. Cardoso, M.C. Oliveira, E.A. Leite, D. Rubello, A.L.B. Barros, Paclitaxel-loaded folate-coated long circulating and pH-sensitive liposomes as a potential drug delivery system: a biodistribution study, Biomed. Pharmacother. 97 (2018) 489–495, https://doi.org/10.1016/j.biopha.2017.10.135.
[31] L.O.F. Monteiro, R.S. Fernandes, L. Castro, D. Reis, G.D. Cassali, F. Evangelista, C. Loures, A.P. Sabino, V. Cardoso, M.C. Oliveira, A.B. Barros, E.A. Leite, Paclitaxel-Loaded folate-coated ph-sensitive liposomes enhance cellular uptake and antitumor activity, Mol. Pharm. 16 (2019) 3477–3488, https://doi.org/10.1021/acs.molpharmaceut.9b00329.
[32] J.O. Silva, R.S. Fernandes, C.M.R. Oda, T.H. Ferreira, A.F.M. Botelho, M.M. Melo, M.C. Miranda, D.A. Gomes, G.D. Cassali, D.M. Townsend, D. Rubello, M. C. Oliveira, A.L.B. Barros, Folate-coated, long-circulating and pH-sensitive liposomes enhance doxorubicin antitumor effect in a breast cancer animal model, Biomed. Pharmacother. 118 (2019), 109323, https://doi.org/10.1016/j.biopha.2019.109323.
[33] G. Haran, R. Cohen, L.K. Bar, Y. Barenholz, Transmembrane ammonium sulfate gradients in liposomes produce efficient and stable entrapment of amphipathic weak bases, Biochim. Biophys. Acta Biomembr. 1151 (1993) 201–215, https://doi.org/10.1016/0005-2736(93)90105-9.
[34] M.S. Oliveira, S.V. Mussi, D.A. Gomes, M.I. Yoshida, F. Frezard, V.M. Carregal, L.A. M. Ferreira, 5α-Tocopherol succinate improves encapsulation and anticancer activity of doxorubicin loaded in solid lipid nanoparticles, Colloids Surf. B 164 (2016) 243–256, https://doi.org/10.1016/j.colsurfb.2015.12.019.
[35] V. Vichai, K. Kirtikara, Sulforhodamine B colorimetric assay for cytotoxicity screening, Nat. Protoc. 1 (2006) 1112–1116, https://doi.org/10.1038/nprot.2006.179.
[36] R.S. Fernandes, J.O. Silva, H.A. Seabra, M.S. Oliveira, V.M. Carregal, J.M.C. Vilela, M.S. Andrade, D.M. Townsend, P.M. Colletti, A. Elaine, V.N. Leite, L.A.M. Cardoso, D. Ferreira, A.L.B. Rubello, Barros, 7α- Tocopherol succinate loaded nano-structed lipid carriers improves antitumor activity of doxorubicin in breast cancer models in vivo, Biomed. Pharmacother. 103 (2018) 1348–1354, https://doi.org/10.1016/j.biopha.2018.04.139.
[37] C.C.F. Faraco, J.A.Q.A. Faria, M. Kunrath-Lima, M.C. Miranda, M.I.A. Melo, A. F. Ferreira, M.A. Rodrigues, D.A. Gomes, Translocation of Epidermal Growth Factor (EGF) to the nucleus has distinct kinetics between adipose tissue-derived mesenchymal stem cells and a mesenchymal cancer cell lineage, J. Struct. Biol. 202 (2018) 61–69, https://doi.org/10.1016/j.jsb.2017.12.007.
[38] Organization For Economic Co-Operation And Development (OECD). Guideline for Testing of Chemicals 423: Acute Oral Toxicity – Acute Toxic Class Method, 2001.
[39] W. Xu, J. Ding, C. Xiao, L. Li, X. Zhuang, X. Chen, Versatile preparation of intracellular-acidity-sensitive oxime-linked polysaccharide-doxorubicin conjugate for malignancy therapeutic, Biomaterials 54 (2015) 72–86, https://doi.org/10.1016/j.biomaterials.2015.03.021.
[40] N. Kramer, A. Walzl, C. Unger, M. Rosner, G. Krupitza, M. Hengstschläger, H. Dolznig, In vitro cell migration and invasion assays, Mutat. Res. Rev. Mutat. Res. 753 (2013) 10–24, https://doi.org/10.1016/j.mrrev.2012.08.001.
[41] J.S. Basuki, H.T.T. Duong, A. Macmillan, R.B. Erlich, L. Esser, M.C. Akerfeldt, R. M. Whan, M. Kavallaris, C. Boyer, T.P. Davis, Using fluorescence lifetime imaging microscopy to monitor theranostic nanoparticle uptake and intracellular doxorubicin release, ACS Nano 7 (2013) 10175–10189, https://doi.org/10.1021/nn404407g.
[42] Y. Barenholz, S. Amselem, D. Goren, R. Cohen, D. Gelvan, A. Samuni, E.B. Golden, A. Gabizon, Stability of liposomal doxorubicin formulations: problems and prospects, Med. Res. Rev. 13 (1993) 449–491, https://doi.org/10.1002/med.2610130404.
[43] D.S. Ferreira, S.D. Faria, S.C.A. Lopes, C.S. Teixeira, A. Malachias, R. Magalhães-Paniago, J.D. Souz-Filho, B.L.J.P. Oliveira, A.R. Guimarães, P. Caravan, L.A. M. Ferreira, R.J. Alves, M.C. Oliveira, Development of a bone-targeted pH-sensitive liposomal formulation containing doxorubicin: physicochemical characterization,

cytotoxicity, and biodistribution evaluation in a mouse model of bone metastasis, Int. J. Nanomed. 11 (2016) 3737–3751, https://doi.org/10.2147/IJN.S109966.
[44] M.C. Woodle, L.R. Collins, E. Sponsler, N. Kossovsky, D. Papahadjopoulos, F. J. Martin, Sterically stabilized liposomes. Reduction in electrophoretic mobility but not electrostatic surface potential, Biophys. J. 61 (1992) 902–910, https://doi.org/10.1016/S0006-3495(92)81897-0.
[45] S.C.A. Lopes, M.V.M. Novais, C. S. T, K. Honorato-Sampaio, M.T. Pereira, L.A. M. Ferreira, F.C. Braga, M.C. Oliveira, Preparation, physicochemical characterization, and cell viability evaluation of long-circulating and pH-sensitive liposomes containing ursolic acid, Biomed. Res. Int. 2013 (2013), 467147, https://doi.org/10.1155/2013/467147.
[46] S.A. Abraham, D.N. Waterhouse, L.D. Mayer, P.R. Cullis, T.D. Madden, M.B. Bally, The liposomal formulation of doxorubicin, Methods Enzymol. 391 (2005) 71–79, https://doi.org/10.1016/S0076-6879(05)91004-5.
[47] N. Muhamad, T. Plengsuriyakarn, K. Na-Bangchang, Application of active targeting nanoparticle delivery system for chemotherapeutic drugs and traditional/herbal medicines in cancer therapy: a systematic review, Int. J. Nanomed. 13 (2018) 3921–3935, https://doi.org/10.2147/IJN.S165210.
[48] C. Müller, R. Schibli, Prospects in folate receptor-targeted radionuclide therapy, Front. Oncol. 3 (2013) 329, https://doi.org/10.3389/fonc.2013.00249.
[49] M. Scaranti, E. Cojocaru, S. Banerjee, U. Banerji, Exploiting the folate receptor α in oncology, Nat. Rev. Clin. Oncol. 17 (2013) 349–359, https://doi.org/10.1038/s41571-020-0339-5.
[50] F. Tavassolian, G. Kamalinia, H. Rouhani, M. Amini, S.N. Ostad, M.R. Khoshayand, F. Atyabi, M.R. Tehrani, R. Dinarvand, Targeted poly (L-γ-glutamyl glutamine) nanoparticles of docetaxel against folate over-expressed breast cancer cells, Int. J. Pharm. 467 (2014) 123–138, https://doi.org/10.1016/j.ijpharm.2014.03.033.
[51] A. Akbarian, M. Ebtekar, N. Pakravan, Z.M. Hassan, Folate receptor alpha targeted delivery of artemether to breast cancer cells with folate-decorated human serum albumin nanoparticles, Int. J. Biol. Macromol. 152 (2020) 90–101, https://doi.org/10.1016/j.ijbiomac.2020.02.106.
[52] J. Kazi, R. Sen, S. Ganguly, T. Jha, S. Ganguly, M.C. Debnath, Folate decorated epigallocatechin-3-gallate (EGCG) loaded PLGA nanoparticles; in-vitro and in-vivo targeting efficacy against MDA-MB-231 tumor xenograft, Int. J. Pharm. 585 (2020), 119449, https://doi.org/10.1016/j.ijpharm.2020.119449.
[53] M.S. Jhaveri, A.S. Rait, K. Chung, J.B. Trepel, E.H. Chang, Antisense oligonucleotides targeted to the human alpha folate receptor inhibit breast cancer cell growth and sensitize the cells to doxorubicin treatment, Mol. Cancer Ther. 3 (2004) 1505–1512.
[54] J.P. Marshalek, P.S. Sheeran, P. Ingram, P.A. Dayton, R.S. Witte, T.O. Matsunaga, Intracellular delivery and ultrasonic activation of folate receptor-targeted phase-change contrast agents in breast cancer cells in vitro, J. Control. Release 243 (2016) 69–77, https://doi.org/10.1016/j.jconrel.2016.09.010.
[55] H. Banu, D.K. Sethi, A. Edgar, A. Sheriff, N. Rayees, N. Renuka, S.M. Faheem, K. Premkumar, G. Vasanthakumar, Doxorubicin loaded polymeric gold nanoparticles targeted to human folate receptor upon laser photothermal therapy potentiates chemotherapy in breast cancer cell lines, J. Photochem. Photobiol. B 149 (2015) 116–128, https://doi.org/10.1016/j.jphotobiol.2015.05.008.
[56] C.A.P. Monteiro, A.D.P.R. Oliveira, R.C. Silva, R.R.M. Lima, F.O. Souto, M. O. Baratti, H.F. Carvalho, B.S. Santos, P.E. Cabral-Filho, A. Fontes, Evaluating internalization and recycling of folate receptors in breast cancer cells using quantum dots, J. Photochem. Photobiol. B 209 (2020), 111918, https://doi.org/10.1016/j.jphotobiol.2020.111918.
[57] P. Kumar, P. Huo, B. Liu, Formulation strategies for folate-targeted liposomes and their biomedical applications, Pharmaceutics 11 (2019) 381, https://doi.org/10.3390/pharmaceutics11080381.
[58] J.M. Horacek, M. Vasatova, R. Pudil, M. Tichy, P. Zak, M. Jakl, L. Jebavy, J. Maly, Biomarkers for the early detection of anthracycline-induced cardiotoxicity: current status, Biomed. Pap. Med. Fac. Univ. Palacky. Olomouc Czech Republic 158 (2014) 511–517, https://doi.org/10.5507/bp.2014.004.
[59] C. Tien, Y. Peng, F. Yang, Y. Subeq, R. Lee, Slow infusion rate of doxorubicin induces higher pro-inflammatory cytokine production, Regul. Toxicol. Pharmacol. 81 (2016) 69–76, https://doi.org/10.1016/j.yrtph.2016.08.002.
[60] O. Tacar, P. Sriamornsak, C.R. Dass, Doxorubicin: an update on anticancer molecular action, toxicity and novel drug delivery systems, J. Pharm. Pharmacol. 65 (2013) 157–170, https://doi.org/10.1111/j.2042-7158.2012.01567.x.
[61] K.E. O'Connell, A.M. Mikkola, A.M. Stepanek, A. Vernet, C.D. Hall, C.C. Sun, E. Yildirim, J.F. Staropoli, J.T. Lee, D.E. Brown, Practical murine hematopathology: a comparative review and implications for research, Comp. Med. 65 (2015) 96–113.
[62] Z. Su, J. Ye, Z. Qin, X. Ding, Protective effects of madecassoside against Doxorubicin induced nephrotoxicity in vivo and in vitro, Sci. Rep. 14 (2015) 1–14, https://doi.org/10.1038/srep18314.
[63] D. Bengaied, A. Ribeiro, M. Amri, D. Scherman, P. Arnaud, Reduction of hepatotoxicity induced by doxorubicin, J. Integr. Oncol. 6 (2017) 1–12, https://doi.org/10.4172/2329-6771.1000193.
[64] K. Razavi-Azarkhiavi, A.H. Jafarian, K. Abnous, B.M. Razavi, K. Shirani, M. Zeinali, M.R. Jaafari, G. Karimi, The comparison of biodistribution, efficacy and toxicity of two PEGylated liposomal doxorubicin formulations in mice bearing C-26 colon carcinoma: a preclinical study, Drug. Res. 66 (2016) 330–336, https://doi.org/10.1055/s-0035-1569447.
[65] V.W.S. Lee, D.C.H. Harris, Adriamycin nephropathy: a model of focal segmental glomerulosclerosis, Nephrology 16 (2011) 30–38, https://doi.org/10.1111/j.1440-1797.2010.01383.x.
[66] M.M.M. Refaie, E.F. Amin, N.F. El-Tahawy, A.M. Abdelrahman, Possible protective effect of diacerein on doxorubicin-induced nephrotoxicity in rats, J. Toxicol. 2016 (2016), 9507563, https://doi.org/10.1155/2016/9507563.
[67] R. Luo, Y. Li, M. He, H. Zhang, H. Yuan, M. Johnson, M. Palmisano, S. Zhou, D. Sun, Distinct biodistribution of doxorubicin and the altered dispositions mediated by different liposomal formulations, Int. J. Pharm. 519 (2017) 1–10, https://doi.org/10.1016/j.ijpharm.2017.01.002.
[68] R.S. Fernandes, J.O. Silva, S.C.A. Lopes, S. Chondrogiannis, D. Rubello, V. N. Cardoso, M.C. Oliveira, L.A.M. Ferreira, A.L.B. Barros, Technetium-99m-labeled doxorubicin as an imaging probe for murine breast tumor (4T1 cell line) identification, Nucl. Med. Commun. 37 (2016) 307–312, https://doi.org/10.1097/MNM.0000000000000443.